

PAPER • OPEN ACCESS

Morphological investigation of maleic anhydride-grafted nitrile/nanoclay nanocomposites

To cite this article: Mohamed Zemzem *et al* 2022 *Mater. Res. Express* **9** 085302

View the [article online](#) for updates and enhancements.

You may also like

- [Mechanical and thermal characterization of functionalized maleic anhydride grafted polypropylene](#)
Mohammad Y Al-Haik, Waseem Siddique, Mohammad M Kabir *et al.*
- [The study on composites formation from HDPE and sawdust/rice husk as raw materials](#)
F Mulana, M Mariana, M N Hadman *et al.*
- [A novel reverse osmosis membrane modified by polyvinyl alcohol with maleic anhydride crosslinking](#)
Mohit Samnani, Harshad Rathod and Hiren Raval



EDINBURGH INSTRUMENTS

WORLD LEADING MOLECULAR SPECTROSCOPY SOLUTIONS

edinst.com

The advertisement features a red background with the Edinburgh Instruments logo on the left, which consists of a circular pattern of white dots. In the center, there are several pieces of laboratory equipment, including a spectrophotometer labeled 'F55', a larger instrument labeled 'F55', and a fluorescence spectrometer labeled 'FLS 1000'. The text 'WORLD LEADING MOLECULAR SPECTROSCOPY SOLUTIONS' is written in white, bold, uppercase letters. The website 'edinst.com' is displayed in a white box in the bottom right corner.



PAPER

Morphological investigation of maleic anhydride-grafted nitrile/nanoclay nanocomposites

OPEN ACCESS

RECEIVED

28 April 2022

REVISED

23 July 2022

ACCEPTED FOR PUBLICATION

2 August 2022

PUBLISHED

10 August 2022

Original content from this work may be used under the terms of the [Creative Commons Attribution 4.0 licence](#).

Any further distribution of this work must maintain attribution to the author(s) and the title of the work, journal citation and DOI.

Mohamed Zemzem¹ , Ludwig Vinches² and Stéphane Hallé¹¹ Dept. of Mechanical Engineering, École de Technologie Supérieure 1100 Notre-Dame West, Montreal (QC) H3C 1K3, Canada² Dept of Environmental Health and Occupational Health, University of Montreal 2375, Chemin de la Côte Sainte-Catherine, Montreal (QC) H3T 1A8, CanadaE-mail: mohamed.zemzem.1@ens.etsmtl.ca**Keywords:** nitrile rubber, layered silicate nanoparticles, maleic anhydride, rubber/clay nanocomposite, exfoliation and orientation**Abstract**

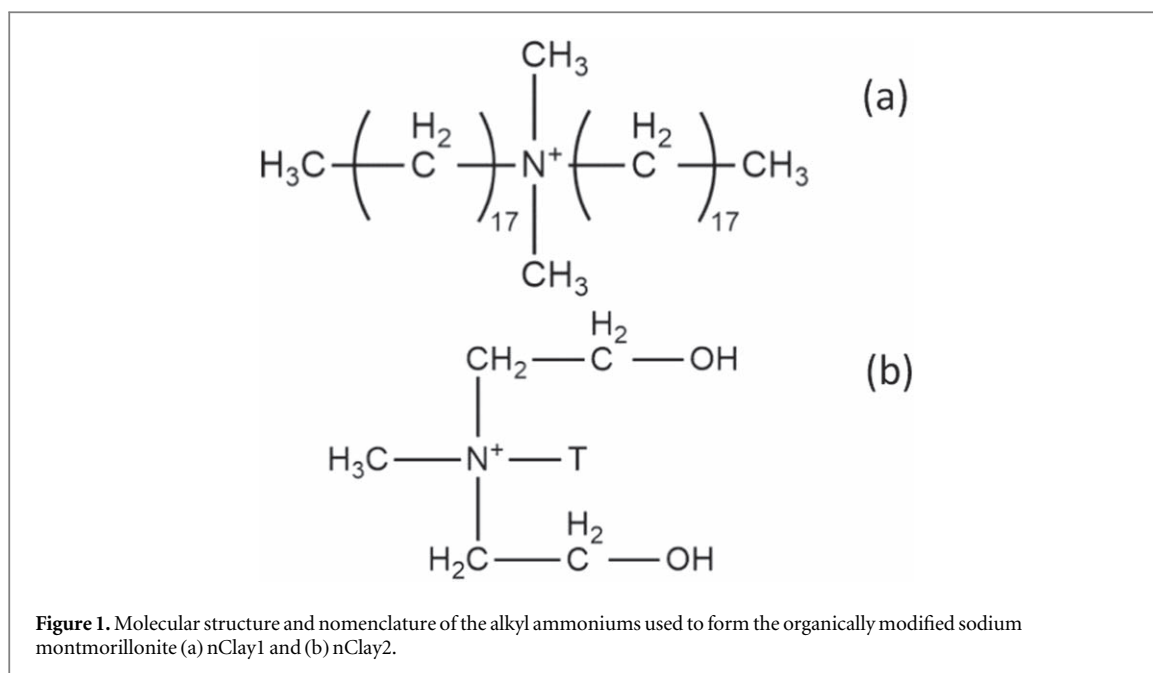
The dispersion and orientation of three different montmorillonite clay nanoparticles embedded in nitrile-based nanocomposites were examined in the current study. Maleic anhydride was grafted onto a nitrile structure for the purpose of enhancing compatibility, and the resulting nanocomposites were investigated. The grafting of maleic anhydride seemed to have a pronounced effect, leading the structure to a near-exfoliation state. Using energy dispersive x-ray spectrometer, the state of distribution of layered silicate clusters in the nanocomposite was assessed, and it was observed that maleic anhydride provided a reduction in the size of agglomerations and enhanced the homogeneity of the system. The intercalation and delamination of the layered silicates over grafting were validated by transmission electron microscopy. Inter-lamellar spacing measurements were found to correlate perfectly with x-ray data. On the other hand, the alignment of the clay nanoparticles was examined by small angle x-ray scattering. A 3D-orientation approach was developed based on the scattering stereographs.

Introduction

Polymer/nano-filler nanocomposites have attracted considerable attention for both industrial and scientific applications due to their unique capacity to exhibit enhanced characteristics and value-added qualities over unfilled virgin polymers [1, 2]. Their synergistic properties were of concern for substantial material characteristics such as enhancing barrier properties, increasing mechanical moduli [3], and improving flame retardancy [4]. Of all the nano-fillers tested for their reinforcing ability, clay nanoparticles have gained momentum due to their availability, low cost, intrinsic anisotropy, and their impressive capacity to tune polymer properties at considerably low loading concentrations [5]. Nano-clays (nClays) belong to the class of layered mineral materials and were termed as stacks of silicate sheets (nano-platelets) approximately 1 nm in thickness and up to several microns of lateral dimensions.

To date, chemical casting and melt compounding have been considered as ranking among the most efficient techniques for processing nanocomposites [6, 7]. However, physically mixing a polymer with layered silicate nanoparticles may not systematically lead to a nanocomposite. The presence of nClays as agglomerated tactoids or clusters of layers within the matrix would provide poor reinforcing ability, making it comparable to conventional microcomposites. The key factor for achieving a successful nanocomposite is to obtain a homogeneous dispersion and good distribution of separated individual layers in the polymeric matrix. In [8], it was found, however, that achieving a complete separation of nano-platelets is quite challenging because of the presence of interlayer ionic bonds. Moreover, the difference in polarity in the nClays/polymer system implies weak interfacial interaction, rendering complete dispersion more difficult.

In order to enhance the affinity between nanoclays and the polymeric matrix, a naturally hydrophilic silicate surface could be rendered organophilic by implementing organic cations on the surface of the layers [9]. Many studies have found that adding reactive functional groups to the organic modifier further enhances compatibility



in the nanocomposite system. Polar molecules, such as maleic anhydride, grafted onto the polymeric backbone have been found to lower the interfacial energy and improve the wetting properties of the system [10, 11]. Chemical affinity causes the infiltration of polymeric macromolecules into the nClays' host galleries, leading to an increase in the interlayer spacing. Appropriate processing parameters, along with a proper chemical tailoring, could lead the nanocomposite to a high level of dispersion and a state of near-exfoliation. Further, some authors have highlighted a particularly attractive design involving the preferred alignment of the layered silicates in the material. [12, 13] found that the nano-platelet orientation provides rigidity, stiffness, and bi-dimensional stability to the polymer.

A lot of interest has been directed at nanocomposites based on thermoplastic polymers. Morphological studies, as well as investigations of their industrial properties, have been examined thoroughly. However, except for some studies that have been conducted in the field of rubber/nanoclay systems [14–16], few attempts have been undertaken to understand the morphology of elastomeric nanocomposites.

The present article aims to provide an understanding of the dispersion and alignment of layered silicates within their associated nanocomposites. The effects of organic modification on nanoparticles and of maleic anhydride grafting on rubber are depicted by cross-checking various characterization techniques.

Reagents and materials

Acrylonitrile-butadiene rubber (NBR) was selected as an elastomeric matrix for the investigated nanocomposite materials. Powdered NBR under the trade name of Baymod N34.52 and containing 34% acrylonitrile was provided by Matexion (ON, Canada). ACS-grade acetone used for sample dissolution in chemical casting procedures was purchased from Fisher Scientific. Maleic anhydride (MA) and benzoyl peroxide (BPO) were both acquired from Aldrich Chemical. BPO was used as an initiator for the grafting of MA onto the nitrile rubber.

Three commercial grades of clay nanoparticles were purchased from Sigma-Aldrich. The nClays were labeled based on whether they were unmodified (nClay/0) or had chemical modifications applied to the surface of their nano-platelets (nClay/1 and nClay/2). nClay/0 is a natural inorganic sodium montmorillonite (Na + MMT) with the chemical formula $(\text{Na}, \text{Ca})_{0.33}(\text{Al}, \text{Mg})_2(\text{Si}_4\text{O}_{10})(\text{OH})_2 \cdot n\text{H}_2\text{O}$. nClay/1 is a montmorillonite clay chemically modified with about 35 to 45 wt% dimethyl dialkyl (C14-C18) amine. nClay/2 is also a natural montmorillonite modified with 30 wt% methyl hydroxyethyl tallow (T) ammonium. The tallow structure is ~65% C18, ~30% C16, and ~5% C14. The organoclays were investigated to assess the effects of surface modification on the dispersion of the nClay platelets in the elastomeric matrix. Figure 1 shows the chemical structures of amine surfactants that were exchanged for the sodium ion of the native montmorillonite clay and used to form the organoclays nClay/1 and nClay/2.

Methodology

Nanocomposite preparation

Nitrile rubber nanocomposites containing the described clay nanoparticles were prepared. The concentration of the filler was held constant at 5% for all samples. The following processing techniques were adopted to obtain an optimal configuration of the nClays dispersion. It is worth noting that prior to every preparation, all powders were oven-dried at 65 °C for 24 h.

Solution mixing

Rubber/clay nanocomposites were synthesized by a solution-intercalation casting method. NBR powder was dissolved in acetone at 60 °C. The ratio of the rubber to solvent was 2:5 weight/volume. The solution was continuously stirred using a magnetic stirrer at 700 rpm for 20 h until complete dissolution. On the other hand, 5 parts of nClay powder per hundred parts of rubber were added under constant stirring and dispersed in acetone at a 1:30 weight/volume ratio. The same stirring and temperature conditions were maintained for 20 h. Prior to rubber/nanoparticle solution mixing, the nClay solution was ultra-sonicated using a UIP1000hd ultrasonic processor (Hielscher ultrasound tech) for 30 min at 60 °C. The ultra-sonication frequency was set to 20 kHz to ensure a better delamination of the nClay platelets and a standard 0.5-diameter flat horn tip was used. Subsequently, both solutions were mixed and stirred with a high shear hydrodynamic dispersion process for an additional 30 min at 6000 rpm using a Silverson L5M-A Laboratory High Shear Mixer. The resulting solution was then cast over in a thoroughly cleaned sheet of Teflon to avoid sticking issues. The sample was kept in ambient condition under a ventilated hood until the evaporation of most of the solvent. The obtained film was then vacuum-dried in the oven for 24h at 60 °C–70 °C for a complete drive-out of residual acetone.

Melt processing

To guarantee a better distribution, the prescribed amounts of nClays were premixed with the rubber by shaking in a sealed glass container. Melt processing was then conducted in two steps. The powdered compound was melt-mixed in a Brabender mixer equipped with twin roller blades (Rheomix OS). For all samples, mixing was conducted at 135 °C for 5 min. Compounding speed was set at 100 rpm. The resulting mixture was retrieved from the mixing chamber, cooled at room temperature, then pelletized in a grinder for the next processing step. The pellets were extruded using a Haake PolyLab OS—RheoDrive 4 co-rotating twin screw extruder (Rheomix OS PTW16). The rotation speed was set at 100 rpm. The barrel and the flat-die temperature profile ranged from 150° to 160 °C.

Preparation of maleated nanocomposites

The preparation of maleated nanocomposite rubber was carried out in two stages; grafted nitrile rubber was firstly prepared by grafting NBR with maleic anhydride in the presence of benzoyl peroxide in a Brabender mixer. One part per hundred rubber (phr) was pre-mixed with nitrile powder for 5 min at 80 °C and 100 rpm. 2 phr of MA was then added for an additional 5 min under the same mixing conditions. The resulting mixture was then extruded in accordance with the procedure described in the previous section.

The nomenclature adopted to label the nanocomposites under study was as follows. Each nanocomposite was appointed as RCN/xy-5% where x stood for the nature of the nClay (0, 1 and 2 for nClay/0, nClay/1 and nClay/2, respectively) and y referred to the processing technique (1 for solution casting and 2 for melt processing). The same terminology was used for the maleated sample with an extra g for grafting (RCNg/xy-5%). One of the prepared nanocomposites was quenched with liquid nitrogen right after extrusion. For the quenched sample, a letter q was used (RCNq/xy-5%)

Afterward, all compounds were press-molded in the form of sheets of 125 × 125 × 2 mm at 150 °C under 10 MPa pressure using a hydraulic press in accordance with ASTM Standard D3187–06 [17]. Curing time was defined by the rheological data obtained from a MCR 501 Anton Paar rheometer.

Nanocomposites structural characterization methods

Fourier transform IR spectroscopy analysis

The infrared (IR) spectra were recorded on a Perkin-Elmer FTIR-ATR Spectrometer from 4000 to 400 cm⁻¹ with an average of 5 scans and at a resolution of 1 cm⁻¹. For the analysis of the as-received powdered clay nanoparticles, 100 to 200 mg samples were disc-shaped using a hand-held press for 5 s at room temperature. On the other side, grafted and non-grafted nanocomposite samples were processed in a 1 mm thick film by hot pressing.

X-ray diffraction experiments

The morphology properties of the nanoparticles, as well as the synthesized rubber nanocomposites, were investigated at room temperature by an x-ray diffractometer (XRD - Philips PANalytical X'pert PRO). The layered silicate galleries basal spacing (d-spacing) was monitored using a nickel-filtered $\text{CuK}\alpha$ radiation at a generator voltage of 45 kV and a wavelength of $\lambda = 1.541 \text{ \AA}$. The diffraction curves were obtained within the range of scattering angles (2θ) of $2.5\text{--}10^\circ$ and at a scan rate of $1^\circ \cdot \text{min}^{-1}$. The d-spacing was calculated according to Bragg's equation.

Scanning electron microscopy and energy dispersive x-ray spectroscopy studies

Agglomerations and clusters of clay nanoparticles could be detected with ultra-high-resolution scanning electron microscopy (UHR-SEM). Observations were conducted using a Hitachi SU-8230 SEM using an accelerating voltage of 5 kV. Cross-sections of 1 mm-thick nanocomposite films were observed. Samples were microtomed by a Leica (RM2235) cryo-microtome at -100°C using a tungsten knife, then coated with a 2 nm-thick platinum layer.

Given the capability of the electron microscope to detect nanoclay clusters down to a few tens of nanometers, the energy dispersive x-ray (EDX) module coupled to the UHR-SEM was adopted to detect characteristic chemical elements of the nanoclays. Therefore, the EDX technique was employed to establish a statistical study about the look of the cluster's size distribution as a function of the nanocomposite composition as well as the nClays' nature. Measurements were acquired in bi-dimensional mapping mode at a count rate of 100 kcps and for a scan time of 120 s. Size distribution assessment was based on averaging data collected from five different spots for each specimen. The analysis was done at a working distance of around 15 mm and with a magnification of 5K for each one of the spots. The count of the agglomerations and the evaluation of their area for size distribution calculations were established in post-treatment using the ImageJ software.

Transmission electron microscopy observations

Further inspection of the state of dispersion of the nClays platelets in the elastomeric matrix came from transmission electron microscopy analysis. Observations were carried out using an FEI Tecnai G2 F20 TEM equipped with a Gatan Ultrascan 4000 $4k \times 4k$ CCD Camera System Model 895 EDAX Octane T Ultra W /Apollo XLT2 SDD and TEAM EDS Analysis System operating at 200 kV. Samples as thin as 50–100 nm were cut from the cross-section of nanocomposite films at -120°C using a Leica Microsystems UC7/FC7 cryo-ultramicrotome equipped with a diamond knife. Fractured sections were transferred from the knife edge onto coated 200-mesh copper grids.

Small angle x-ray scattering measurements

To investigate nClay orientation in the nanocomposite material, Small angle x-ray diffraction experiments (SAXS) were conducted. A Bruker Nanostar diffractometer was adopted with a pinhole geometry camera using a 2D wire detector at 28 cm of distance between the sample and the detector. Further, a representation of the 3D orientation of the nClays platelets was constructed based on 2D SAXS patterns taken from the three Cartesian directions of a 1 mm cubic sample with respect to the incident x-ray beam.

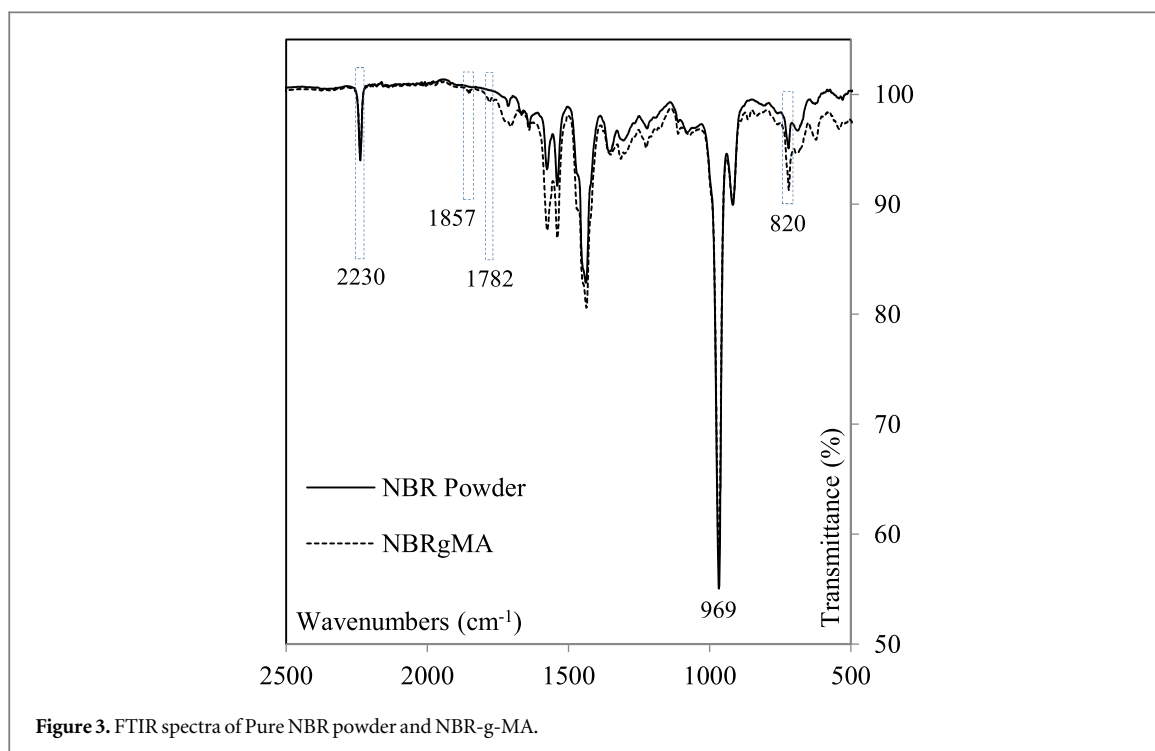
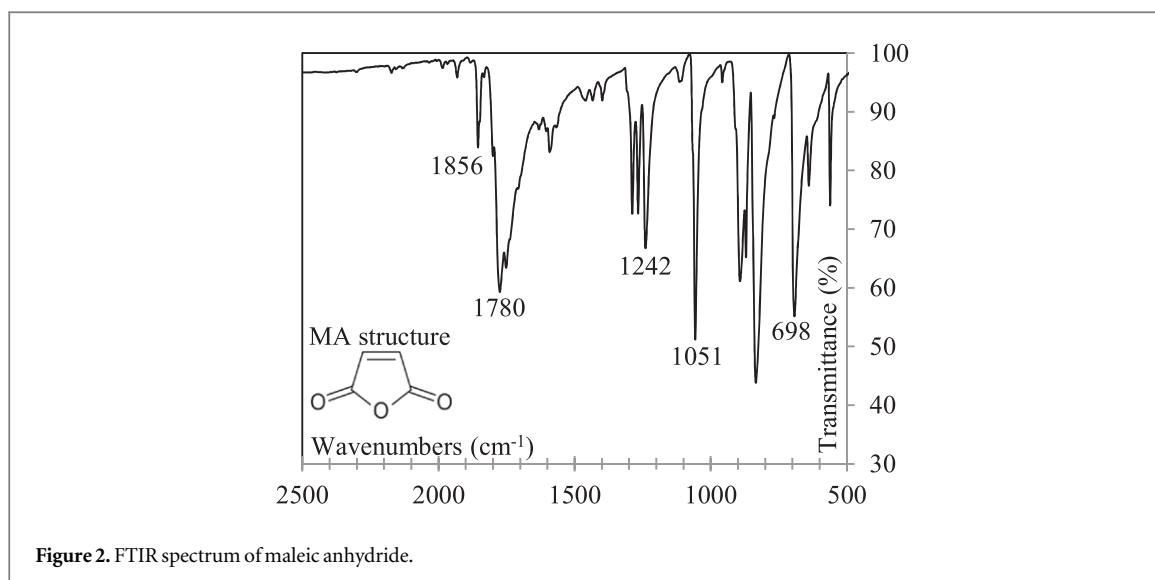
Results and discussions

MA grafting assessment with FTIR

Maleic anhydride was chosen as a grafted monomer for its high double reactivity. Chemical anchoring of the reactive monomer on the NBR backbone can be examined by identifying the grafting sites using FT infrared spectroscopy [18, 19]. In the beginning, absorption made by the major bonds in the MA structure was depicted. Figure 2 shows the FTIR spectrum of row maleic anhydride. The plot exhibited well-defined peaks at 1856 cm^{-1} and 1780 cm^{-1} . Those signals were assigned to the asymmetric and symmetric stretching of carbonyl ($\text{C}=\text{O}$) groups located at the cyclic anhydride, respectively [20]. Asymmetric and symmetric ring stretching of the groups ($=\text{C}-\text{O}-\text{C}=\text{O}$), unique to the cyclic ethers, were also clearly spotted at 1242 cm^{-1} and 1051 cm^{-1} , respectively. From the opposite side of the monomeric structure, a relatively broad peak, noticed at around 698 cm^{-1} , was identified as the stretching of the olefinic bond ($\text{C}=\text{C}$) [21].

To properly investigate MA-grafting on the NBR structure, it is mandatory to figure out the mechanism of grafting and understand the transformation that the MA monomer undergoes after the process. Grafting of maleic anhydride may either occur on the polyacrylonitrile or the poly-butadiene segments of a given rubber containing these elements [22].

Figure 3 represents plots of IR spectrum of the rubber/clay nanocomposite grafted with MA compared to the spectrum of the Pure NBR.



First, it could be noticed that new absorption peaks at around 1782 and 1857 cm^{-1} were observed. These signals were assigned to the strong symmetric and weak asymmetric stretching absorption of the carbonyl group ($\text{C}=\text{O}$) characteristic of the cyclic succinic anhydride [23]. Moreover, the grafting of MA is achieved by the creation of a free radical in the position of the double carbon bond of the monomer. Indeed, the absorbance of the ($\text{C}=\text{C}$) signal considerably reduced in the NBR-g-MA spectrum giving place to ($\text{C}-\text{C}$) bond. It should be mentioned, however, that the peak didn't completely disappear which suggested the presence of some unreacted MA present in the blend [19, 21]. The MA was thus successfully introduced as a graft onto the rubbery structure. The relatively weak signal of the peaks is due to the low concentration of MA in the compound (2%). For grafting on the acrylonitrile segment of the copolymeric backbone, MA monomer would occur by addition on the unsaturated triple bond of the cyano group ($\text{C}\equiv\text{N}$). However, by inspecting the FTIR spectrum of the NBR-g-MA and compare it to the NBR signal, no decrease was noticed at the absorbance site of the cyano group located at 2230 cm^{-1} and the triple bond was unaffected. This is suggesting that grafting would rather happen on the butadiene part of the backbone. Besides, anchoring of MA in the butadiene region could take place either by the formation of a vinylic radical monomer through abstraction and substitution of a hydrogen atom from a vinylic position, or by an addition of this monomer to the carbon double bond as a result of an Ene-reaction [24, 25].

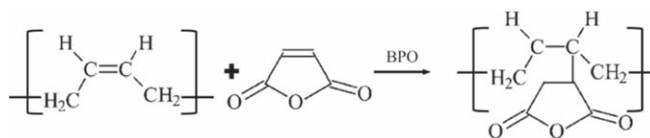


Figure 4. Possible grafting reaction product of polybutadiene and maleic anhydride.

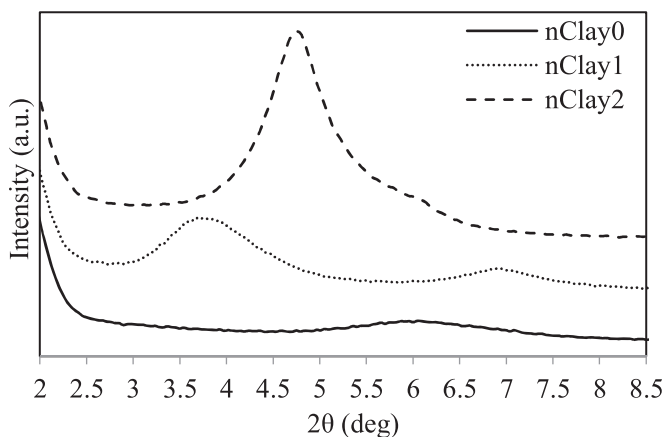


Figure 5. XRD patterns of MMT Bentonite Na + (nClay/0), MMT treated with dimethyl dialkyl quaternary ammonium (nClay/1), and MMT treated with methyl tallow bis-2-hydroxyethyl quaternary ammonium (nClay/2).

By examining the IR spectra, it was noticed that the absorbance represented by the strong and sharp peak located at 969 cm^{-1} remained unchanged after addition of MA to the rubber. This signal corresponds to the absorbance caused by the (C–H) out of plane bending vibrations. Thus, the result reduced the probabilities that the monomer could be grafted by the substitution of vinylic hydrogen in the polybutadiene (PB) segment [22]. On the other hand, a slight decrease in intensity was spotted on the absorbance above 820 cm^{-1} . The aforementioned peak matches with the vibrations of the carbon double bond (C=C) on the polybutadiene section. Therefore, it can be deduced that there are high chances that MA grafting could occur on the double bond of the PB [25]. Accordingly, the grafting reaction during melt processing would possibly take place according to the reaction portrayed in figure 4.

X-ray diffraction analysis of the nClay dispersion

Chemical treatment of nClay layers by cation exchange results in an enlargement of the interlayer spacing. X-ray diffraction measurements of the nClays investigated in this study were plotted as Intensity versus 2θ curves in figure 5. XRD spectrum of the untreated montmorillonite nanoclay showed a broad peak located at the diffraction angle $2\theta = 6^\circ$, similar findings are reported in the literature [26]. This diffraction corresponds to a basal spacing (d-spacing) of 14.73 \AA according to Bragg's law applied to a diffraction emitted from a copper source. This spacing is caused by the presence of moisture attracted by the cationic charges located in the interlayers, as previously described in the thermal analysis section. nClay/1, treated with dimethyl dialkyl quaternary ammonium surfactant, exhibited a well-defined reflection at $2\theta = 3.71^\circ$ corresponding to a d-spacing of 23.82 \AA . A second, less noticeable peak was spotted at $2\theta = 6.9^\circ$ (d-spacing 12.81 \AA). Both signals were related to the scattering of the (001) and (002) plans of the layered stacks, respectively [27]. Regarding nClay/2, which was treated with methyl tallow di-hydroxyethyl quaternary ammonium surfactant, a single peak positioned at a diffraction angle of $2\theta = 4.79^\circ$ (d-spacing 18.45 \AA) was identified and assigned to the reflection of the plan (001). Therefore, surface modification applied to nClay/1 and nClay/2 increased basal spacing of the first plan by about 60 and 25 percent, respectively. The variation in the d-spacing could be related to the extent of the nano-layers surface area occupied by the organic surfactants. In fact, authors like Younghonn and al. [28] attempted to estimate the organic surface area based on calculations of the cation exchange capacity of the nClays, which is $92\text{ meq}/100\text{g}$ for sodium MMT, and molecular dimensions of the surfactants. It was deduced that the quaternary ammonium cations of nClay/1 and nClay/2 cover about 120% and 70% of the layers surface, respectively. In addition, the number of long alkyl chains in the surfactants was found to affect the interlayer space in the nClays (two in nClay/1 versus one in nClay/2) [28, 29].

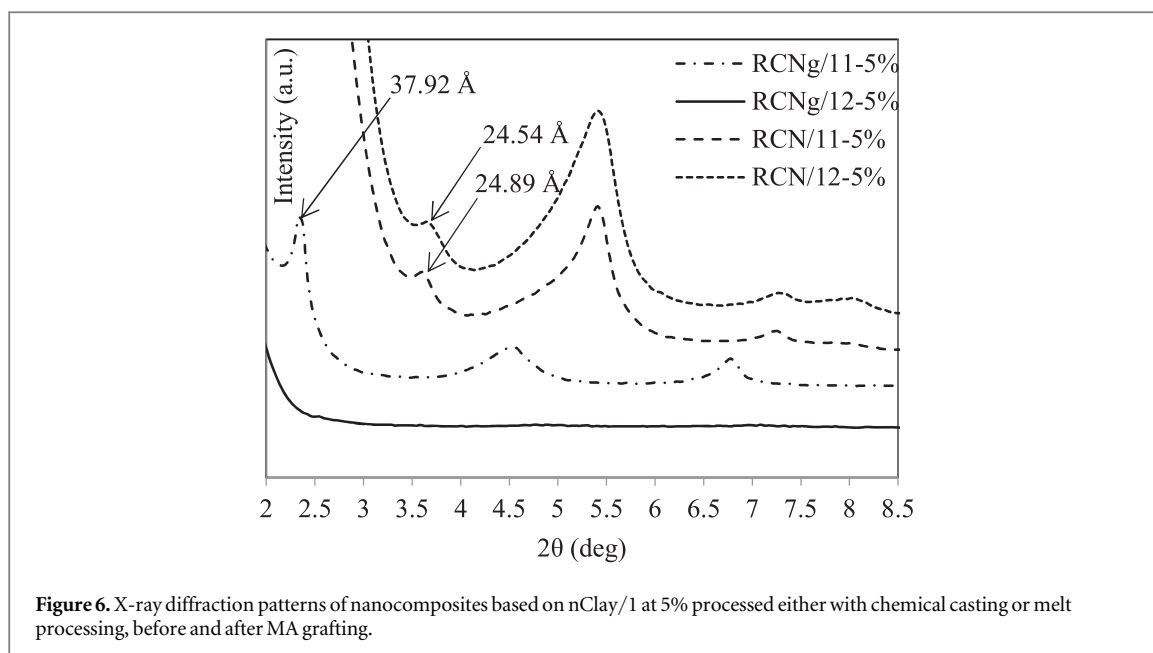


Table 1. Basal spacing corresponding to the (001) plane reflection of nClay/0 and nClay/2 within the nitrile nanocomposites.

Nanocomposite	d-spacing (Å)	Nanocomposite	d-spacing (Å)
RCN/01%–5%	N/A	RCN/21%–5%	23.88
RCN/02%–5%	N/A	RCN/22%–5%	24.21
RCNg/01%–5%	No peak	RCNg/21%–5%	No peak
RCNg/02%–5%	No peak	RCNg/22%–5%	No peak

In the next step, shape and position of the basal reflections in the XRD spectra were investigated to probe the nanocomposites morphology and occasionally to monitor the extent of dispersion of the nano-platelets in the rubbery matrix. Diffraction patterns of various rubber/nClays hybrids based on nClay/1 are portrayed in figure 6. It should be mentioned that the marked peaks in the figure refer to the basal reflection of the plane (001) of the nClay/1. Peaks appearing at higher diffraction angles were found to be caused by some crystalline structures located in the pure nitrile rubber as mentioned in a previous study [30]. Regarding the unmaleated nanocomposites RCN/11%–5% and RCN/12%–5%, the position of the nClay/1 scattering was slightly shifted to the lower angles suggesting an expansion of the montmorillonite layers of about 1.07 Å and 0.72 Å, respectively. The variation of the nClay/1 layers d-spacing inside the NBR matrix was barely noticeable. The hypothesis of polymeric chains intercalation in the inter-lamellar voids is very unlikely. The literature rather attributed a small increase of basal spacing to a rearrangement of the surfactants long alkyl molecules located in the interlayer spaces [31]. From another standpoint, a more significant increase in d-spacing was seen with nClay/2 over fabrication with both processing methods. From table 1 (curves not shown), an expansion of the order of 5.76 Å and 5.43 Å were reported with RCN/21%–5% and RCN/22%–5% respectively. Therefore, the incorporation of nClay/2 nanoparticles in nitrile rubber with both chemical casting and melt compounding procedures seemed to result in the penetration of the polymeric chains in between the silicate layers. Accordingly, the change in the peaks positions implies a pronounced inclusion of the rubbery macromolecules within the nClay/2 galleries. Therefore, this inclusion led to the formation of an intercalated nanocomposite [32, 33]. As a matter of fact, the quaternary ammonium surfactant used for the surface treatment of nClay/2 contains hydroxyl groups (O–H) rendering the hydrophilic silicate layers more organophilic [34]. On the other side, the highly polar cyano groups (C≡N) located at the acrylonitrile segment of the nitrile rubber are very likely to establish stable hydrogen bonding with the similarly polar hydroxyl groups [33, 35]. It might be thought then that the enhanced polarity of the silicate layers facilitated the intercalation of the acrylonitrile section, representing 34% of the overall rubber, within the inter-lamellar voids. Note, however, that as long as the reflection peaks were still present in the XRD spectra, a complete separation of the layers and an entire delamination of the tactoids were far from being achieved [36]. For nClay/0, it was quite difficult to distinguish

the peak associated to the nanoparticle from the wavy background associated to the matrix. Unfortunately, no obvious conclusions could be drawn from it.

A common note was observed in melt processed nanocomposites grafted with maleic anhydride with all three nClays under investigation: a clear absence of scattering peaks corresponding to the reflections of nClays interlayer spacing (figure 6 and table 1). It might be assumed that a considerable amount of the layered stacks lost their crystallographic ordering and orientation within the nanocomposites structure [37]. Similar profiles were observed with the nanocomposites from chemical casting, except for RCNg/11%–5% for which a prominent increase of d-spacing of 14.1 Å was recorded. Subsequently, it was deduced that the layered silicates reached a state of near exfoliation regardless of the surface treatment of the nClays and independently of the chemical nature and the size of the surfactant. By consequence, it was presumed that the presence of grafted MA played the major role in the delamination of the silicate layers. Authors working on maleated polyolefins and organophilic nano-clay systems [38] reported a similar conclusion. They showed that the driving forces for polymeric chains penetration in the galleries were hydrophilic interactions in the form of strong hydrogen bonds between –COOH groups located in the MA structure and the structural oxygen present in the silicate layers. The same deduction was stipulated with maleated EPDM and organoclays nanocomposites [30].

From the disappearance of pre-existing peaks of d-spacing reflections a conclusion could be made about the extent of exfoliation of the nClays stacks. Nevertheless, it turns out that the result of having a flat XRD spectrum wouldn't systematically mean getting homogeneous nanocomposite of well dispersed individual layers. By looking at the mechanism of the platelets' separation, two things happen to a given piling of layers. First, since the intercalated macromolecules penetrate randomly inside the galleries, a loss of the platelets stacking order occurs. This, hence, leads to a reduction in the size of the stack and causes a broadening of the corresponding reflection peak in the spectrum [39]. Second, following a fairly wide extent of intercalation, multiple basal d-spacings arise giving birth to a whole distribution of broad and weak diffraction peaks for a given platelets stack [40]. Those factors contribute to the appearing of what looks like smooth flat curves as seen with the maleated nanocomposite in figure 6. Taking into account these considerations, the morphology rather tends to look like clusters of well expended and disordered few-numbered platelets piles. Single layers might also be present because of a delamination mechanism following shear stress applied during melt processing.

SEM observations and EDX assessment of the nClays state of dispersion

Despite the capabilities of the x-ray diffraction analysis to provide convenient understanding about the inter-lamellar spacing of the nClays layers before and after inclusion in the rubber, little can be said about the state of dispersion and the special distribution of the nClays in the elastomeric matrix. Crosschecking with electronic imaging technique would provide a better understanding of the nanocomposite morphology. For the nanoparticles to be perceived in the SEM micrographs, chemical etching was applied to the observed fracture surface to remove the surrounding rubber, pop up the nClays to the surface and create a topology. Figures 7(a.1) and (b.1) display SEM micrographs of RCN based on the untreated nClay/0 before and after MA grafting, respectively. Magnification was set in such a way that the expected size (lateral dimension) of the fillers could be detectable. Well defined profiles could readily be spotted in both images, but no obvious conclusions could be made as to their nature.

Based on the SEM setups, silicate entities could be indirectly detected through elemental analysis of the characteristic x-rays backscattered electrons after a primary electron bombardment of the sample's surface. Measurements were conducted using an energy dispersive x-ray spectrometer coupled to the electron microscope and tuned to the mapping mode. From a chemical point of view, it should be highlighted that the nClays under investigation are synthetic minerals composed of an alumina octahedral layer sandwiched between two tetrahedral silica layers at a ratio of 2:1 [41]. Given the difference in their ionic valence, trivalent aluminum cations are very often partially substituted by bivalent magnesium cations within the silicate layers [42]. Accordingly, Si, Al, and Mg are substantial elements present in the structure of the investigated nClays regardless of the organic surface modification. Those elements are thus characteristic of the nClays and were used as markers to detect the presence of the nanoparticles in the micrographs. As a side note, the platinum signal was originated from the conductive coating applied to the sample and sodium was the exchangeable cation located on the platelet's surface. The best contrast to distinguish the nClays was achieved when elemental mapping of all the three structural elements (Si, Al, and Mg) were superposed in a single image. Such mapping images of nitrile/nClay/0 hybrids before and after MA grafting are jointly shown in figures 7(a.2) and (b.2).

At first glance, the omnipresence of relatively large sizes of well-defined nClay clusters could be seen in the mapping image of the non-grafted nanocomposite. Smaller separated agglomerations could also be spotted in the same image. The blue contrast in-between represents the surrounding rubbery matrix. On the other hand, maleated nanocomposite exhibited a homogeneous pattern of much smaller and uniform nanoparticle agglomerations. Also, it could be noted that the intermediate space showed a brighter contrast compared to the

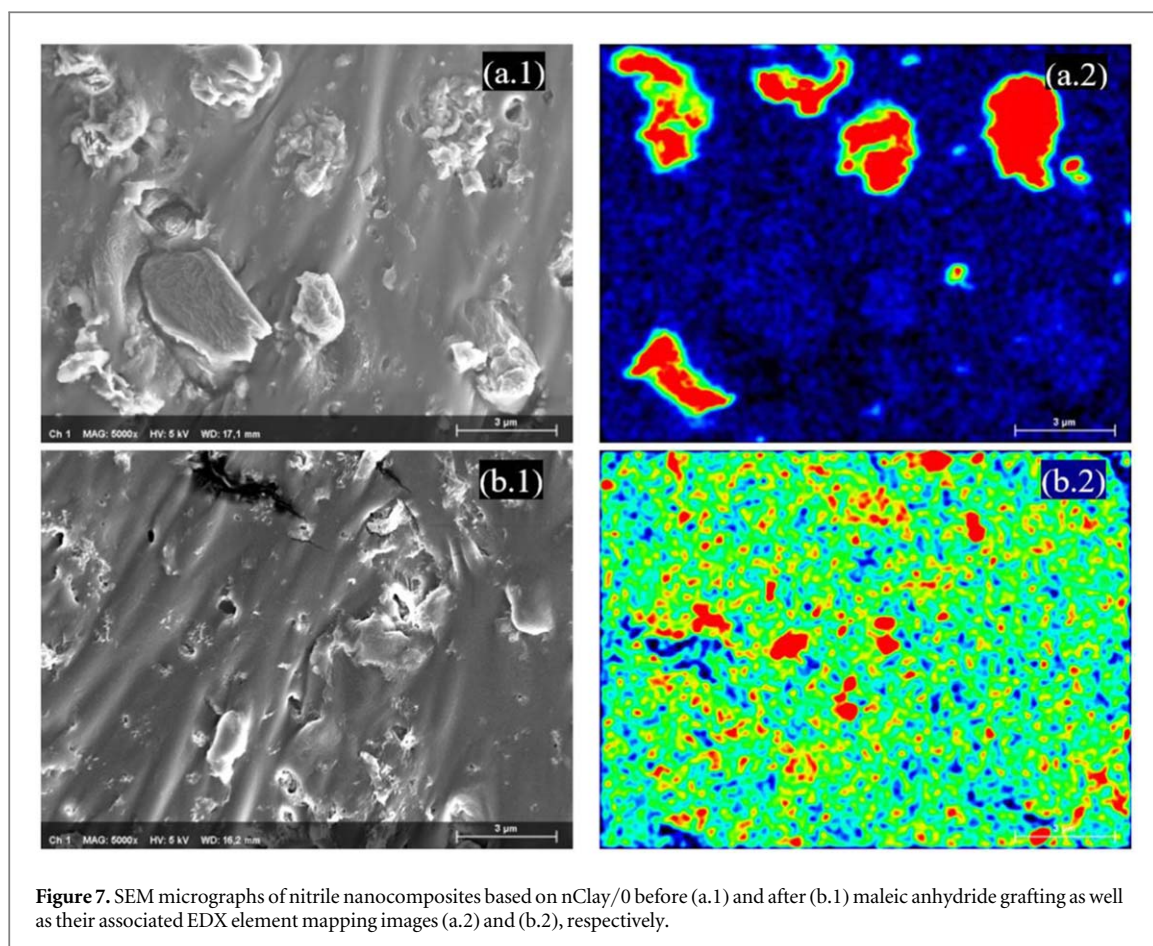


Figure 7. SEM micrographs of nitrile nanocomposites based on nClay/0 before (a.1) and after (b.1) maleic anhydride grafting as well as their associated EDX element mapping images (a.2) and (b.2), respectively.

non-grafted material. This is suggesting either the presence of even smaller silicate entities which were barely detected by the device, or the existence of agglomerations located few microns beneath the probed surface. Either way, this observation connotes an enhancement of the nClays distribution within the nanocomposite. For further investigation, quantitative analysis of size distributions of the agglomerations was conducted. In each nanocomposite, counting was based on data collected from a sum of five mapping images at the same magnification. Since no regular shape was discerned for the agglomerations, assessed size was set to denote the surface area of the entities. A protocol was developed on image editing software (ImageJ) to identify the agglomerations based on their brightness and their contrast in the mapping images. Automated counting was then executed. The formerly described size distribution histograms are depicted in figure 8. Counting results showed that the number of agglomeration entities in the nanocomposites, for the same inspected area, increased by more than 2.5 times after the grafting of MA (from 43 to 111 entities). Additionally, the histogram of the RCN/01%–5% revealed a near-flat distribution. More specifically, almost every size range of $0.05 \mu\text{m}^2$ from 0.01 to $1 \mu\text{m}^2$ contained up to five agglomeration entities. After MA grafting, RCNg/01%–5% exhibited a clear asymmetric peak shifted to the right of the graph and showing that over 30% of the nClays assemblies had a surface area of about $0.05 \mu\text{m}^2$. This finding helped to throw some light on the effects of MA grafting on decreasing the size of the agglomerations and homogenizing the morphology of the RCNs.

TEM experiments

Further characterization support was provided from TEM to allow a localized understanding of the internal morphology of the nClays as well as views of the defect structure [43]. Figures 9(a) and (b) portray TEM bright field micrographs at a magnification of 200K representing nitrile nanocomposites cross-sections before and after grafting of maleic anhydride, respectively. The image corresponding to the non-grafted nanocomposite exhibited a region of about dozens of alternating narrow dark and light bands. The described multilayered feature was assigned to a piling of parallel silicate nano-platelets. The thickness of the dark layers was measured in post-treatment and found to be around 1 nm. The result is in agreement with the structural thickness of a silicate monolayer documented in the literature [44]. Accordingly, the adjacent bright band would correspond to the interlayer gallery. Interestingly, the width of this gap measured at ten different positions in the layered structure was equal to $23.65 \text{ \AA} \pm 0.50 \text{ \AA}$. This measurement is in good agreement with the basal d-spacing previously assessed with XRD (24.54 \AA). Similar TEM micrographs in the literature support the findings [45].

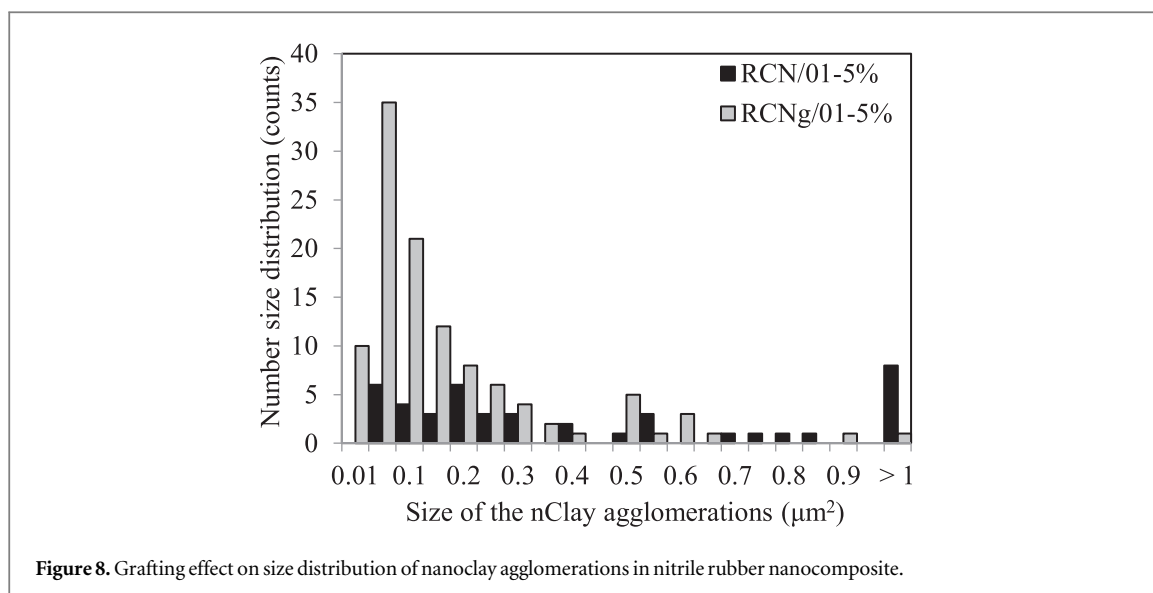


Figure 8. Grafting effect on size distribution of nanoclay agglomerations in nitrile rubber nanocomposite.

It is worth mentioning also that rather than a polymeric intercalation process, dispersion of the layered silicate was additionally undertaken by a delamination mechanism. This phenomenon is reflected in micrographs by the onset separation of small stacks of 2–5 nano-platelets (white arrows) from the external surface of the tactoids. The delamination aspect was repeatedly appearing in several micrographs taken for this nanocomposite. After MA-grafting (figure 9(b)), the existence of separated monolayers was clearly visible in the micrographs being assigned to the single dark hair-like bands.

It is to note though that the overall micrograph was majorly occupied by a bright area corresponding to the rubbery matrix. It must be kept in mind that at this level of magnification, a noticeable inhomogeneity was expected rather than a monolithic morphology.

SAXS experiments for nClay orientation

The orientations of layered silicates in four nanocomposites based on nClay/1 at 5% were examined in this study. Since the processing methods were shown to considerably affect the nClays' alignment, solution cast and melt processed nanocomposites were compared (RCN/11%–5% and RCN/12%–5%). The maleated (RCNg/12%–5%) and quenched (RCNq/12%–5%) nanocomposites were also tested. To get a global overview of the alignment within a tested sample, a technique was adopted to build a three-dimensional representation of the nClays orientation starting from the 2D SAXS patterns. Diffraction results were acquired from the three different directions of a cubic sample. These directions correspond to the machining (MD), tangential (TD), and normal (ND) directions as portrayed in figure 10(a). It should be noted that each one of these directions is perpendicular to its associated plan of diffraction represented by the 2D SAXS stereographs. For the solution casted sample presented in figure 10(b), the 3D scattering spectrograms displayed well defined concentric circles around the primary incident beam. The ring-like dark spots at the first order counting from the center were associated to the 2θ diffraction of the nClays basal d-spacing. Their diffractions agreed with the position of the inter-layers peak reported with XRD. Nearly isotropic patterns in all the directions indicate the existence of randomly orientated nClay platelets within the RCN system [46]. The spectrograms associated to the RCNq/12%–5% and presented in figure 10(c) also showed the reflected intensity of the nClay/1 within the nanocomposite. However, concentric blob-like circles were only spotted from the normal direction. Seen from (MD) and (TD), scattered patterns revealed a lack of diffracted intensities on either side of the central spot. Anisotropic diffraction is the signature of an obvious orientation of the nano-platelets [47]. According to the three-dimensional portrayal, the face and side alignment would suggest an orientation following the line of extrusion during processing. Finally, diffraction patterns of the maleated nanocomposite RCNg/12%–5% were expressed in figure 10(d). As expected, the stereographs exhibited broad diffraction near the central blind spot. No specific scattering could be obviously attributed to the basal d-spacing of the layered silicates.

A convincing approach for determining the three-dimensional orientation of various hierarchical organic and inorganic structures in polymeric systems was described by Bafna and al [48]. This approach was adopted to conduct a more in-depth quantitative investigation of the layered silicate alignment within the nanocomposite samples. As could be deduced from the previous discussion, the presence of periodic lamellar structure such as the nClays was manifested by the appearance of a characteristic ring of scattered intensity at a specific range of diffraction angle 2θ . A curve of intensity versus the azimuthal angle (φ) ranging from 0 to 360° could be plotted

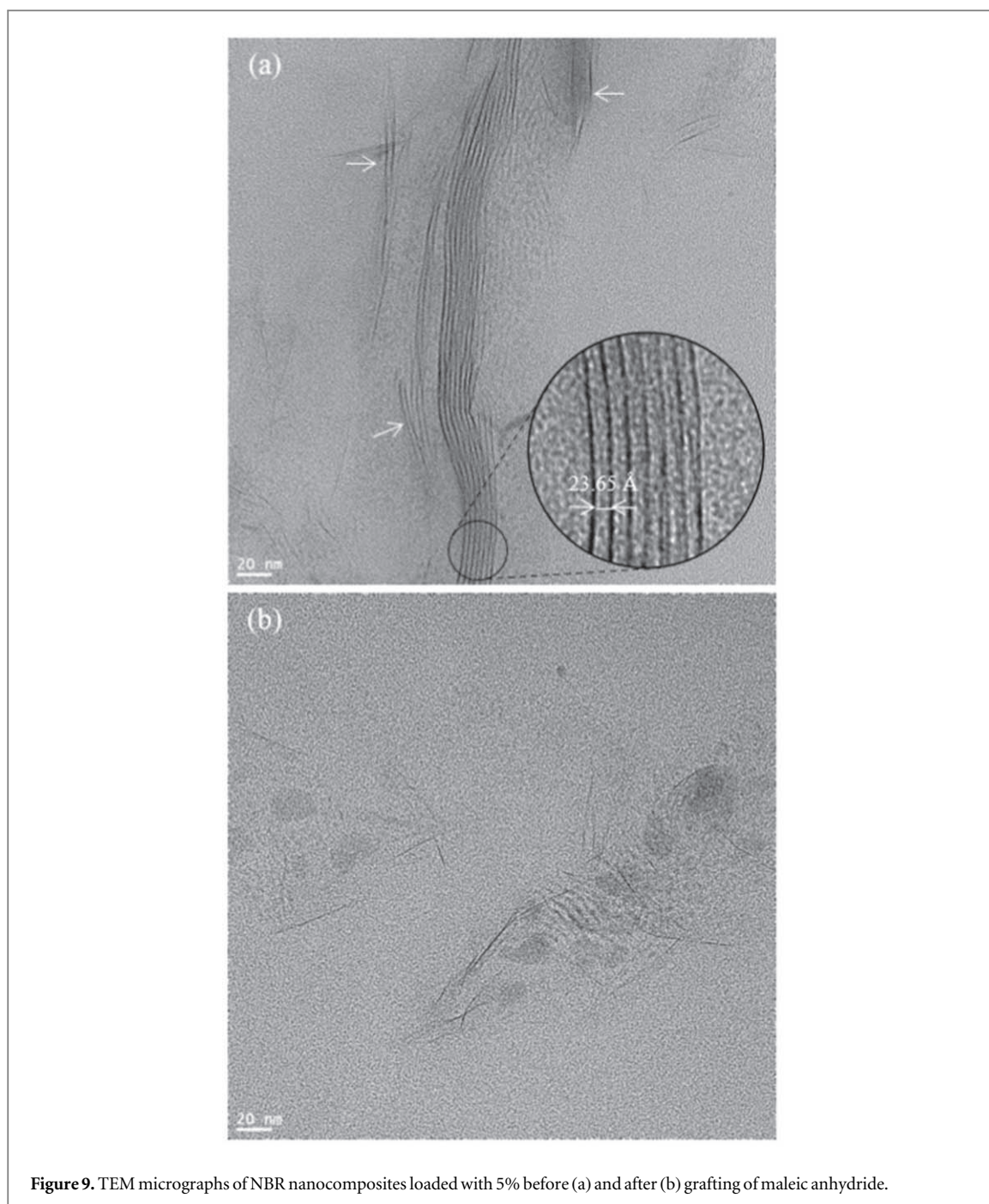


Figure 9. TEM micrographs of NBR nanocomposites loaded with 5% before (a) and after (b) grafting of maleic anhydride.

for each radial position (2θ). In such a curve, the more sharp and intense azimuthal peaks are, the more orientation there is in the structure. For each one of the three previously identified directions, an average cosine square value could be calculated using equation (1) [49] in order to provide a reasonable assumption of the state of alignment distribution of the population of nClays present in the examined nanocomposite sample:

$$\langle \cos^2(\varphi_i) \rangle = \frac{\int_0^{360} I(\varphi_i) \cos^2(\varphi_i) d\varphi_i}{\int_0^{360} I(\varphi_i) d\varphi_i} \quad (1)$$

The letter i stands for directions M, T and N.

The obtained average cosine square value was then used, for each direction i , to assess a so-called Herman's orientation factor (f) given by equation (2) [50]:

$$f_i = \frac{1}{2}(3\langle \cos^2(\varphi_i) \rangle - 1) \quad (2)$$

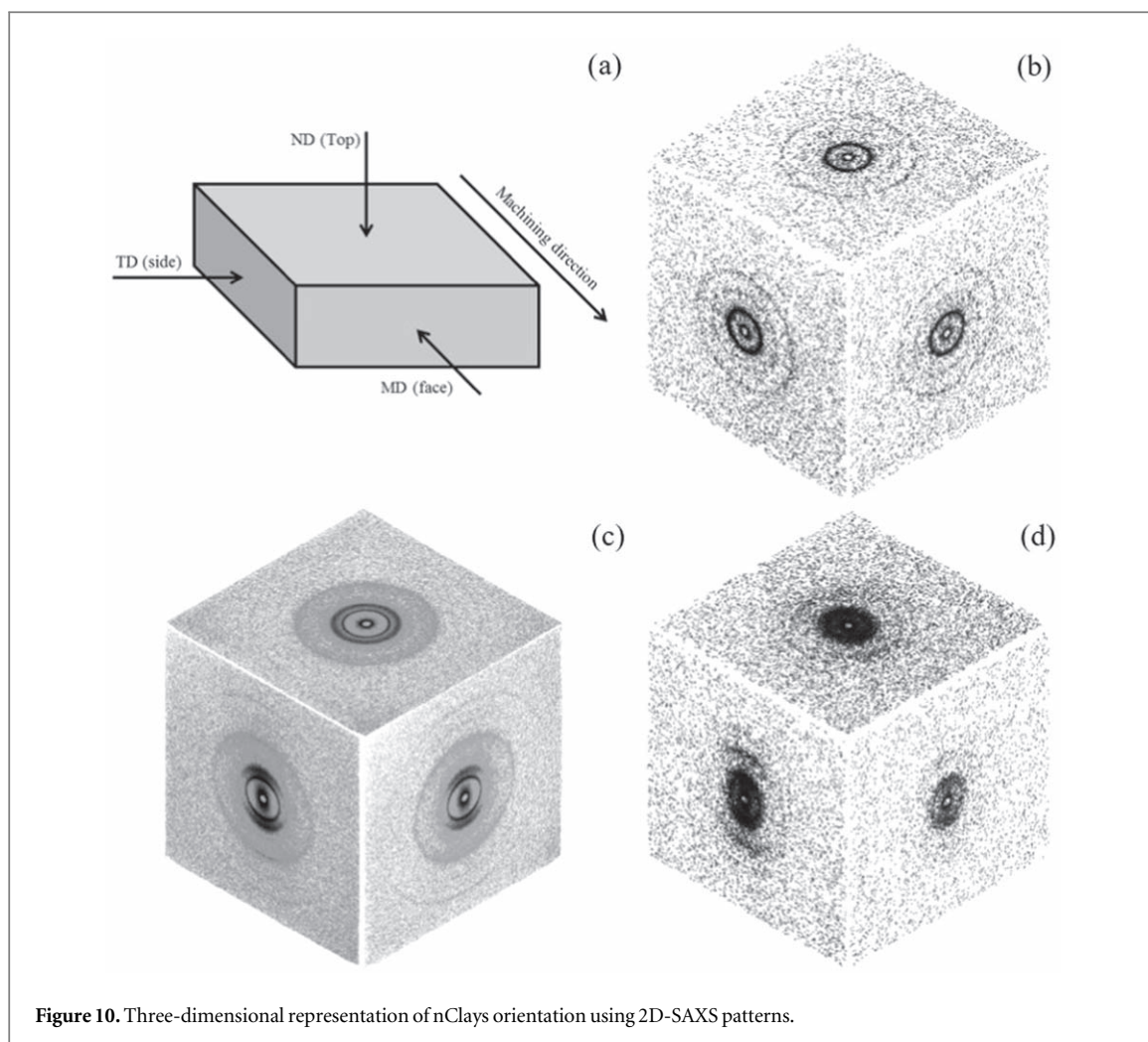
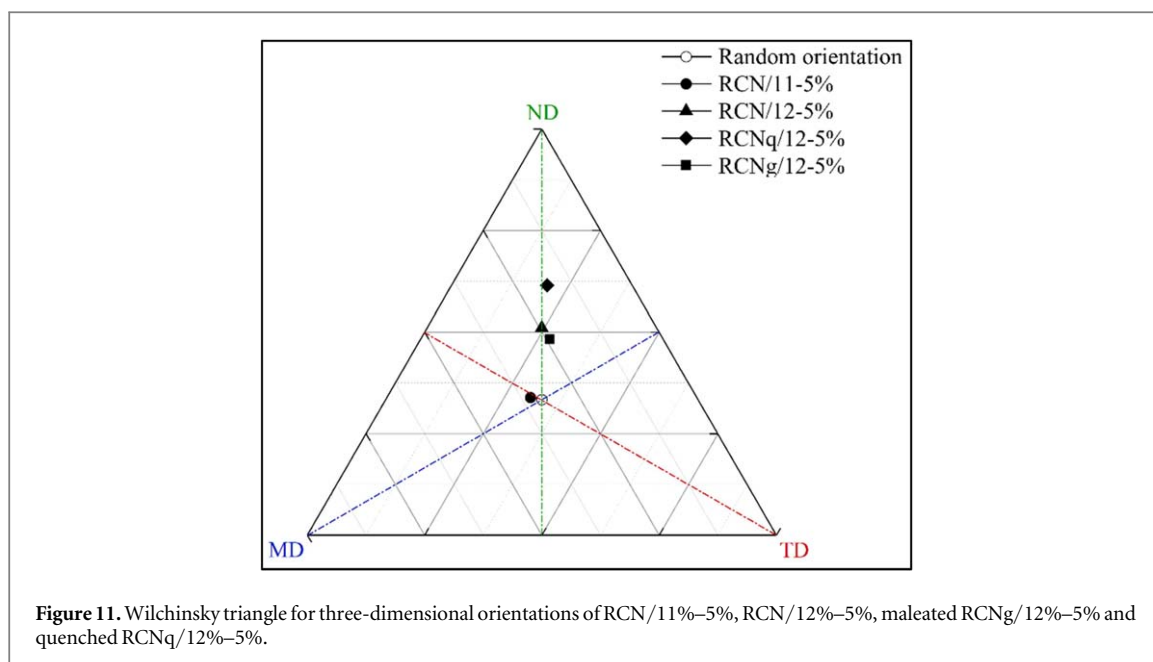


Figure 10. Three-dimensional representation of nClays orientation using 2D-SAXS patterns.

A convenient presentation of the average three-dimensional orientation direction based on Herman's factor data would be by using the Wilchinsky triangle which is a ternary plot that displays the extent of orientation by a single dot [51]. By definition, a completely randomly oriented structure relative to a given direction would have a null Herman's factor, which corresponds to an average cosine square value equal to $1/3$. In this case, the three-dimensional orientation would be represented by a point on the center of the Wilchinsky triangle (unfilled circle in figure 11). On the other hand, the orientation assessment of a structure along a given direction corresponds to the distance of its representative point from the axis of interest for the orientation. In other words, for a structure perfectly orientated in the MT plane, the associated normal direction must be pointed towards the N direction and therefore it would be represented by a point at the ND corner (see figure 11). While an orientation of a structure perpendicularly to the MT plane would be represented by a point on the MT axis opposite to the ND corner.

This approach was adopted to assess the three-dimensional orientation of the four formerly described nanocomposites. The Wilchinsky triangle is portrayed in figure 11. First, it was deduced from the cubic representation of the SAXS stereographs that the chemically casted nanocomposite RCN/11%–5% exhibited an almost totally random 3D orientation within the rubbery system. In fact, its associated point was located very close to the center of the ternary plot. Second, the melt-processed RCN/12%–5% sample showed a point positioned right at the normal to the (MD, MT) axis. That indicates that there was the same extent of orientation in the machining and tangential directions. In addition, this point was located between the center of the triangle and the ND corner. This is suggesting that the layered silicates had an obvious orientation parallel to the MT plane. Third, it could be noticed that the quenched RCNq/12%–5% nanocomposite expressed the same orientation trends compared to RCN/12%–5% but with a corresponding point closer to the ND corner. This was implying a more pronounced orientation parallel to the MT plane. Finally, a point of 3D orientation was associated with the maleated nanocomposite RCNg/12%–5%. The sample followed the same former alignment tendency. However, it is noteworthy that since no well-defined rings were spotted in its corresponding stereographs, the azimuthal curve was constructed from averaging a relatively large range of radial intensity



along the 2θ axis. Therefore, the observed orientation could match better with the alignment of other ordered structures present in the material than the layered nanoparticles.

Conclusions

In summary, the undertaken study was an attempt to design a nitrile-based nanocomposite filled with clay nanoparticles at a high level of dispersion and conducted in a preferred orientation. Layered silicates with organic surface modifications were used to enhance the rubber/filler compatibility. Besides, the rubbery matrix molecules were chemically grafted with maleic anhydride, a highly polar monomer that was expected to improve the affinity between the components and help polymeric chains to intercalate within the nClays galleries. TEM, XRD and EDX/UHR-SEM characterization techniques were combined to build a state of understanding about the homogeneity of the nanocomposites. Grafting with MA was found to provide an astounding improvement to the dispersion of the layered silicates, and a state of near exfoliation was observed. On the other hand, processing the nanocomposites with melt compounding through extrusion was shown to ensure an alignment of the nanoparticles following machining and tangential directions. This arrangement was made clearly noticeable through a 3D orientation approach based on data collected from SAXS. Conclusively, the desired nanocomposite was successfully designed to some extent. It would be of great interest to know if the enhanced structural properties will guarantee improved industrial qualities.

Data availability statement

All data that support the findings of this study are included within the article (and any supplementary files).

Compliance with ethical standards

Conflict of interest

The authors declare that they have no conflict of interest.

Funding

This research did not receive any specific grant from funding agencies in the public, commercial, or not-for-profit sectors. Funding was done entirely based on our in-house budget.

ORCID iDs

Mohamed Zemzem  <https://orcid.org/0000-0001-5508-1360>

References

- [1] Fu S *et al* 2019 Some basic aspects of polymer nanocomposites: a critical review *Nano Materials Science*. **1** 2–30
- [2] Omanović-Miklićanin E *et al* 2020 Nanocomposites: a brief review *Health and Technology*. **10** 51–9
- [3] Zhu T T *et al* 2019 Exfoliation of montmorillonite and related properties of clay/polymer nanocomposites *Appl. Clay Sci.* **169** 48–66
- [4] Yue X *et al* 2019 Flame retardant nanocomposites based on 2D layered nanomaterials: a review *J. Mater. Sci.* **54** 13070–105
- [5] Abulyazied D E and Ene A 2021 An investigative study on the progress of nanoclay-reinforced polymers: preparation, properties, and applications: a review *Polymers*. **13** 4401
- [6] Müller K *et al* 2017 Review on the processing and properties of polymer nanocomposites and nanocoatings and their applications in the packaging, automotive and solar energy fields *Nanomaterials*. **7** 74
- [7] Valapa R B *et al* 2017 *An overview of polymer–clay nanocomposites, Clay-Polymer Nanocomposites* (Amsterdam: Elsevier) 29–81
- [8] Penaloza D P Jr 2019 Modified clay for the synthesis of clay-based nanocomposites *Epitoanyag-Journal of Silicate Based & Composite Materials*. **71** 1
- [9] Perelomov L *et al* 2021 The synthesis of organoclays based on clay minerals with different structural expansion capacities *Minerals* **11** 707
- [10] Dike A S and Yilmazer U 2020 Improvement of organoclay dispersion into polystyrene-based nanocomposites by incorporation of SBS and maleic anhydride-grafted SBS *J. Thermoplast. Compos. Mater.* **33** 554–74
- [11] Moustafa H *et al* 2017 Influence of the degree of exfoliation of an organoclay on the flame-retardant properties of cross-linked ethylene-co-propylene-co-diene monomer-g-Maleic anhydride-based composites *Polym. Compos.* **38** 966–73
- [12] Dhieb F B *et al* 2019 Effect of nanoclay orientation on oxygen barrier properties of LbL nanocomposite coated films *RSC Adv.* **9** 1632–41
- [13] Abdelwahab M *et al* 2020 Studies on the dimensional stability and mechanical properties of nanobiocomposites from polyamide 6-filled with biocarbon and nanoclay hybrid systems *Composites Part A: Applied Science and Manufacturing* **129** 105695
- [14] Kanny K and Mohan T 2017 Rubber nanocomposites with nanoclay as the filler *Progress in Rubber Nanocomposites* (Amsterdam: Elsevier) 153–77
- [15] Zachariah A K *et al* 2019 Vulcanization kinetics and mechanical properties of organically modified nanoclay incorporated natural and chlorobutyl rubber nanocomposites *Polym. Test.* **76** 154–65
- [16] Alobad Z K, Habeeb S A and Albozahid M A 2020 A review on silicone rubber/montmorillonite nanocomposites *The Iraqi Journal for Mechanical and Materials Engineering*. **20** 268–81 (<https://ijfmmme.com/index.php/jmme/article/view/517>)
- [17] ASTM Standard D3187-06 2016 Standard Test Methods for Rubber—Evaluation of NBR (Acrylonitrile-Butadiene Rubber) *ASTM International* (<https://doi.org/10.1520/D3187-06R16>)
- [18] Sclavons M *et al* 1996 The anhydride content of some commercial PP-g-MA: FTIR and titration *J. Appl. Polym. Sci.* **62** 1205–10
- [19] Sclavons M *et al* 2000 Quantification of the maleic anhydride grafted onto polypropylene by chemical and viscosimetric titrations, and FTIR spectroscopy *Polymer* **41** 1989–99
- [20] Sclavons M *et al* 2005 Maleic anhydride-grafted polypropylene: FTIR study of a model polymer grafted by ene-reaction *Polymer* **46** 8062–7
- [21] Nakason C, Kaesaman A and Supasanthitkul P 2004 The grafting of maleic anhydride onto natural rubber *Polym. Test.* **23** 35–41
- [22] Rao B M, Rao P R and Sreenivasulu B 1999 Grafting of maleic anhydride onto acrylonitrile-butadiene-styrene terpolymer: Synthesis and characterization *Polym.-Plast. Technol. Eng.* **38** 967–77
- [23] Yang L *et al* 2003 Microstructure of maleic anhydride grafted polyethylene by high-resolution solution-state NMR and FTIR spectroscopy *Macromolecules* **36** 4709–18
- [24] Lawson D F, Hergenrother W L and Matlock M G 1990 Preparation and characterization of heterophase blends of polycaprolactam and hydrogenated polydienes *J. Appl. Polym. Sci.* **39** 2331–52
- [25] Huang N J and Sundberg D C 1995 Fundamental studies of grafting reactions in free radical copolymerization. III. Grafting of styrene, acrylate, and methacrylate monomers onto cis-polybutadiene using benzoyl peroxide initiator in solution polymerization *J. Polym. Sci., Part A: Polym. Chem.* **33** 2571–86
- [26] Namazi H, Dadkhah A and Mosadegh M 2012 New biopolymer nanocomposite of starch-graft polystyrene/montmorillonite clay prepared through emulsion polymerization method *J. Polym. Environ.* **20** 794–800
- [27] Das A *et al* 2008 Effect of vulcanization ingredients on the intercalation-exfoliation process of layered silicate in an acrylonitrile butadiene rubber matrix *Macromol. Mater. Eng.* **293** 479–90
- [28] Kim Y and White J L 2005 Formation of polymer nanocomposites with various organoclays *J. Appl. Polym. Sci.* **96** 1888–96
- [29] Williams-Daryn S and Thomas R 2002 The intercalation of a vermiculite by cationic surfactants and its subsequent swelling with organic solvents *J. Colloid Interface Sci.* **255** 303–11
- [30] Zemzem M, Vinches L and Hallé S 2018 Influence of processing parameters on barrier properties of nitrile/nanoclay nanocomposite membrane against organic solvent *Journal of Polymer Research* **26** 1–11 (<https://rdcu.be/cTdeJ>)
- [31] Zhou Q *et al* 2007 TEM, XRD, and thermal stability of adsorbed paranitrophenol on DDOAB organoclay *J. Colloid Interface Sci.* **311** 24–37
- [32] Alex R and Nah C 2006 Preparation and characterization of organoclay-rubber nanocomposites via a new route with skim natural rubber latex *J. Appl. Polym. Sci.* **102** 3277–85
- [33] Gatos K G *et al* 2004 Nanocomposite formation in hydrogenated nitrile rubber (HNBR)/organo-montmorillonite as a function of the intercalant type *Macromol. Mater. Eng.* **289** 1079–86
- [34] Ko M B 2000 Effects of acrylonitrile content on the properties of clay-dispersed poly(styrene-co-acrylonitrile) copolymer nanocomposite *Polym. Bull.* **45** 183–90
- [35] Gatos K G *et al* 2005 Controlling the deintercalation in hydrogenated nitrile rubber (HNBR)/organo-montmorillonite nanocomposites by curing with peroxide *Macromol. Rapid Commun.* **26** 915–9
- [36] Teh P *et al* 2004 Effects of epoxidized natural rubber as a compatibilizer in melt compounded natural rubber–organoclay nanocomposites *Eur. Polym. J.* **40** 2513–21

- [37] Lim Y T and Park O O 2001 Phase morphology and rheological behavior of polymer/layered silicate nanocomposites *Rheol. Acta* **40** 220–9
- [38] Hasegawa N and Usuki A 2004 Silicate layer exfoliation in polyolefin/clay nanocomposites based on maleic anhydride modified polyolefins and organophilic clay *J. Appl. Polym. Sci.* **93** 464–70
- [39] Vaia R A et al 1996 Microstructural evolution of melt intercalated polymer–organically modified layered silicates nanocomposites *Chem. Mater.* **8** 2628–35
- [40] Reichert P et al 1998 Nanocomposites based on a synthetic layer silicate and polyamide-12 *Acta Polym.* **49** 116–23
- [41] García-López D et al 2010 Effect of organic modification of sepiolite for PA 6 polymer/organoclay nanocomposites *Compos. Sci. Technol.* **70** 1429–36
- [42] Paul D and Robeson L M 2008 Polymer nanotechnology: nanocomposites *Polymer* **49** 3187–204
- [43] Ray S S and Okamoto M 2003 Polymer/layered silicate nanocomposites: a review from preparation to processing *Prog. Polym. Sci.* **28** 1539–641
- [44] Alexandre M and Dubois P 2000 Polymer-layered silicate nanocomposites: preparation, properties and uses of a new class of materials *Materials Science and Engineering: R: Reports.* **28** 1–63
- [45] Gilman J W 1999 Flammability and thermal stability studies of polymer layered-silicate (clay) nanocomposites1 *Appl. Clay Sci.* **15** 31–49
- [46] Prasad A et al 2001 Morphological study of HDPE blown films by SAXS, SEM and TEM: a relationship between the melt elasticity parameter and lamellae orientation *Polymer* **42** 3103–13
- [47] Alonso R H et al 2009 Nafion–clay nanocomposite membranes: morphology and properties *Polymer* **50** 2402–10
- [48] Bafna A et al 2003 3D hierarchical orientation in polymer–clay nanocomposite films *Polymer* **44** 1103–15
- [49] Bafna A et al 2001 Optical properties and orientation in polyethylene blown films *J. Polym. Sci., Part B: Polym. Phys.* **39** 2923–36
- [50] Vainio U 2016 A size-independent law to describe the alignment of shape-anisotropic objects. arXiv preprint arXiv <https://arxiv.org/abs/1604.05156v1>
- [51] Roe R-J 2000 *Methods of x-ray and neutron scattering in polymer science (Topics in polymer science)*. 9 (Oxford: Oxford University Press) 10–2